

# Cosmic Noise Observation with a Standard Meteor Radar

G. Stober, Ch. Jacobi

## Zusammenfassung

Die Nutzung von Riometern (Relative Ionospheric Opacity Meter) zur Messung relativer atmosphärischer Absorption (in  $dB$ ) ist eine etablierte Methode. Hingegen ist die Messung atmosphärischer Absorption mit absolutkalibrierten Radaren in Form einer Rauschtemperatur eher selten durchgeführt worden. In dieser Arbeit werden die Möglichkeiten einer absoluten Radarkalibrierung für ein kommerzielles SKiYMET-System vorgestellt. Die gemessene QDC (Quiet Day Curve, eine Referenzkurve für ungestörte Tage) wird dabei mit Referenzdaten verglichen. Daran wird der Einfluss des Antennenmusters auf die QDC verdeutlicht und quantitativ dargestellt. Die erreichte Genauigkeit beträgt dabei ungefähr  $600\text{ K}$ . Die kontinuierliche und stabile Beobachtung erlaubt es, die Kopplung der Ionosphäre mit der solaren Aktivität zu untersuchen, ohne den normalen Betrieb zur Meteoranalyse zu unterbrechen.

## Abstract

The observation of relative atmospheric absorption (in  $dB$ ) using Riometers (Relative Ionospheric Opacity Meter) is a well established method. However, the measurement of atmospheric absorption as a noise temperature with absolutely calibrated radars has rarely been realized. This work demonstrates the possibilities to perform an absolute radar calibration for standard SKiYMET meteor radars. The measured QDC (Quiet Day Curve) and the comparison to a reference QDC illustrates the capability to quantify the effect of the antenna pattern. The achieved accuracy for a QDC is approximately  $600\text{ K}$ . The high stability of the observation during normal meteor mode allows also to investigate the ionospheric response caused by the coupling of the solar activity.

## 1 Introduction

Most meteor radars operate in the VHF band, which is within the atmospheric radio window. This means that any transmitted radiation can freely propagate to space. Hence, systems working in this frequency range are also sensitive to cosmic radiation, which is one of the major noise sources for these radars. From Relative Ionospheric Opacity Meter (Riometer) measurements it is known that the cosmic noise signal shows a characteristic pattern according to their geographic latitude and beam tilt (Friedrich et al., 2002). Usually, Riometers observe the extraterrestrial radiation on frequencies between  $20 - 55\text{ MHz}$ . This frequency range is also occupied by standard meteor radars. Unfortunately, the received power  $P$  from the cosmic noise depends on the system frequency and the bandwidth  $B$  of the receiver. Hence, it is more useful to express the received extraterrestrial radiative power as a sky temperature  $T_{sky}$ :

$$P = k_B B T_{sky} \quad , \quad (1)$$

with  $k_B$  as Boltzmann's constant. Another aspect of the cosmic radiation is the effect of ionospheric absorption during times of high ionization rates. This makes such a measurement of the sky temperature sensitive to the solar activity by using an unaffected reference sky temperature map, which can be derived during times of low ionization

operating frequency	36.2 MHz
peak power	4.8 kW
pulse width	12 $\mu$ s
PRF (Pulse Repetition Frequency)	2144 Hz
sampling resolution with 4 point coherent integration	1.87 ms
altitude range	70 – 110 km
altitude gate width	2 km
angular resolution	2°

Table 1: The basic instrumental parameters the radar is operated.

in the MLT (Mesosphere/Lower Thermosphere) region. The differences between the observed sky temperature and those of the reference map give a qualitative ionization level. Thus, it is possible to study day and night as well as summer and winter variations in the background ionization. This is called absorption and often expressed as relative power loss in *dB*. Friedrich et al. (2002) studied the absorption phenomena comparing Riometer measurements with rocket borne wave propagation experiments in the altitude range from 75 to 115 km. Friedrich et al. (2002) expected more than 2/3 of the absorption to occur in this atmospheric region. However, standard meteor radars cover the same frequency range and observe the meteors against the cosmic noise background.

## 2 The Collm meteor radar

The Collm meteor radar (51.3°N,13°E) is a commercially produced SKiYMET all-sky interferometric radar. The system consists of one 3-element Yagi transmitting antenna and five 2-element Yagi receiving antennas. The receiver array is build up as an asymmetric cross with baseline lengths of 2 and 2.5 wavelengths among the receiving antennas. A detailed description of the SKiYMET all-sky meteor radar can be found in Hocking et al. (2001). The basic instrument parameters are given in table 1. It has to be mentioned that the antenna array is placed within a forest and surrounded by trees. The trees have a typical distance among each other of 7 to 9 m. However, during the summer months the receiving antennas are almost completely covered by a roof of leaves from the forest, which leads to additional absorption. The controlling unit is placed in a small barrack 50 m beside the receiving array.

## 3 Cosmic noise sources

There are several sources of extraterrestrial radiation. The basic physical mechanism for the cosmic radio emission are relativistic electrons, which are trapped in strong magnetic fields on spirals orbits. The magnetic fields are created within the galaxies due to their rotation. The electrons move on these spiral orbits with their cyclotron frequency and emit radiation within a cone as predicted by electrodynamic theory. The emitted waves are called synchrotron radiation. The intensity of the emission can be expressed as a radiation temperature  $T_B$  and is described by the Rayleigh-Jeans-law (equation 2). Considering the measured cosmic noise received at a frequency  $\nu$  as black body radiation allows to compute the black body temperature from;

$$T_B = \frac{c^2}{2k_B\nu^2} I_\nu \quad (2)$$

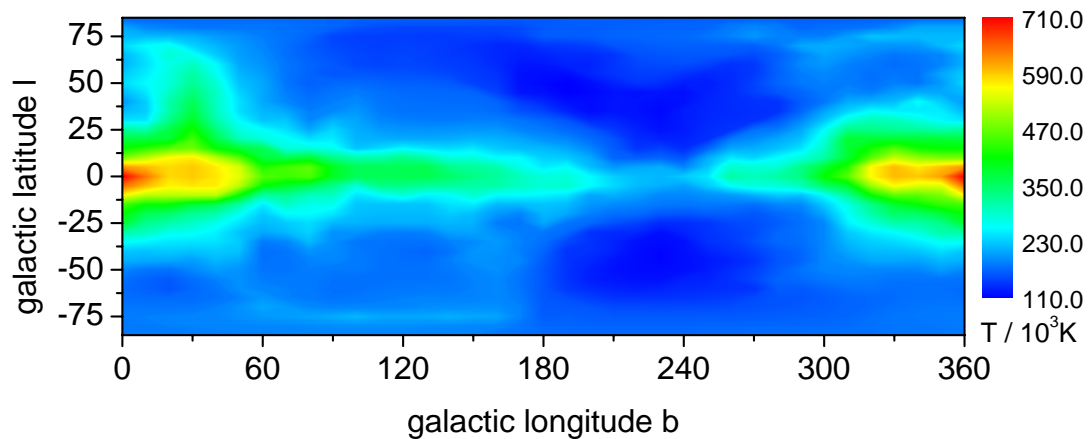


Figure 1: Cane (1978) 30 MHz radio image of our galaxy expressed as a sky temperature. The grid distance is  $10^\circ$  in galactic longitude  $b$  and  $5^\circ$  in galactic latitude  $l$ .

Here  $\nu$  is the frequency,  $I_\nu$  the observed intensity of the radiation,  $c$  the speed of light and  $T_B$  the black body temperature. In figure 1 the sky temperature map derived by Cane (1978) for 30 MHz is given. This map is still the most recent one and illustrated the disc-like structure of our home galaxy. The sky temperature ranges from about 11000 K (low intensity / radio quiet) to 71000 K (high intensity / radio loud). The resolution is  $10^\circ$  in longitude  $b$  [ $0^\circ, 360^\circ$ ] and  $5^\circ$  in latitude  $l$  [ $-85^\circ, 85^\circ$ ]. The red area on the left and right map margin at  $l = \pm 5^\circ$  latitude marks the galactic core. The green area illustrates the galactic disc with reduced radio emission and the blue areas label the areas with a weak contribution to radio noise intensity. For convenience, in figure 2 the map from Cane (1978) is converted to celestial coordinates, which are the more natural coordinates for noise observations with a fixed antenna beam. The grid resolution is again  $10^\circ$  in right ascension  $\alpha$  [ $0^\circ, 360^\circ$ ] and  $5^\circ$  in declination  $\delta$  [ $-85, 85$ ]. Obviously, the galactic core is only visible on the southern hemisphere and the northern hemisphere shows a decreased radio noise intensity. Therefore, one would expect a semidiurnal noise pattern for a radar observing the northern hemisphere and a diurnal pattern for a southern hemispheric measurement. However, the antenna pattern has also to be considered. A large antenna beam width  $\alpha_{eff}$  as used by the SKiYMET can receive cosmic radiation from a widely extended part of the celestial sphere. This can be modeled by using the sky temperature map from Cane (1978) and considering the antenna pattern as well as the geographic latitude. In figure 3 a schematic view of the vertical profile for an antenna beam is shown. The effective opening angle  $\alpha_{eff}$  is defined as the 3 dB power loss compared to the maximum power parallel to the symmetry axis. Some of the Riometers have pivoting antennas to obtain a coverage of different parts on the celestial sphere. However, Friedrich et al. (2002) studied scenarios for non-vertical beams and large F-region electron densities, which can increase the apparent absorption to unrealistic values. As a worst case scenario the absorption can block the complete cosmic radiation emitted from zenith angles above  $70^\circ$ . The same effect limits the opening angles for Riometers and can reduce the effective receiving pattern of the systems. The sky temperature map from Cane (1978) allows to predict a possible QDC in dependence of the radar site, beam tilt and the effective opening angle for an isotropic antenna. The extraterrestrial radiation is important for the meteor radars, as the cosmic background defines the detecting threshold and the minimum measurable electron line density  $q$ . In the following section, it is demonstrated how the cosmic radiation is used to evaluate the antenna calibration.

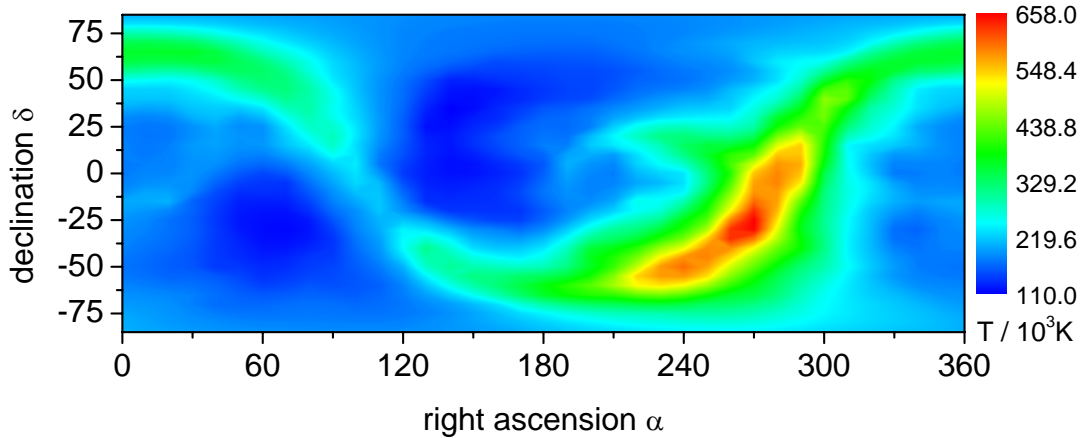


Figure 2: Cane (1978) 30 MHz radio image of our spiral galaxy transformed to celestial coordinates. The grid distance is 10° in right ascension  $\alpha$  and 5° in declination  $\delta$ .

#### 4 Sky temperature measurements - radar calibration

Before a sky temperature can be derived the radar has to be calibrated according to the received power. Usually the receiver measures a voltage  $U$  in digitizer units, which corresponds to a priori unknown power  $P$  in watts;

$$P = c_{cov} \cdot U^2 \quad , \quad (3)$$

where  $c_{cov}$  is a conversion constant, which has to be determined. This procedure is also known as "absolute calibration" and is described in Latteck et al. (2008). However, the basic idea of the calibration is to use the radar volume reflectivity  $\eta$ . The reflectivity is defined as the ration of the total isotropic scattered power to the power density equal to the backscattered radiation, per unit volume and unit incident power density ( Latteck et al., 2008);

$$\eta = \frac{P_r 128 \pi^2 2 \ln(2) r^2}{P_t G_t G_r \lambda^2 e \Theta_{[1/2]}^2 c \tau} \quad , \quad (4)$$

where  $r$  is the scattering range,  $G_t$  and  $G_r$  are the one way antenna gains,  $\Theta_{[1/2]}^2$  is half beam width of the transmitting antenna,  $e$  is the system efficiency including feeding losses,  $P_r$  and  $P_t$  are the received and transmitted power, and  $\tau$  is the pulse width. This equation can be simplified by combining all system dependent variables into one constant;

$$\eta = P_r \cdot c_{cov} \cdot r^2 \quad . \quad (5)$$

This relation already includes the conversion constant  $c_{cov}$  in dependence of the scattering range  $r$ . In principle there are two possibilities to calibrate radars:

- calibration with a calibrated noise source,
- delay line combined with variable attenuation.

In figure 4 both methods are shown schematically. For the calibration the system is switched off and the antenna cables of the transmitter and the receiver are removed. In the case of a delay line calibration the FSU (frequency synthesizer unit) creates the signal for the transmitter, which is then directly fed into the receiver via a delay line of 100  $\mu s$  and an attenuation in the range of 30 dB to 110 dB to avoid the saturation of the receivers.

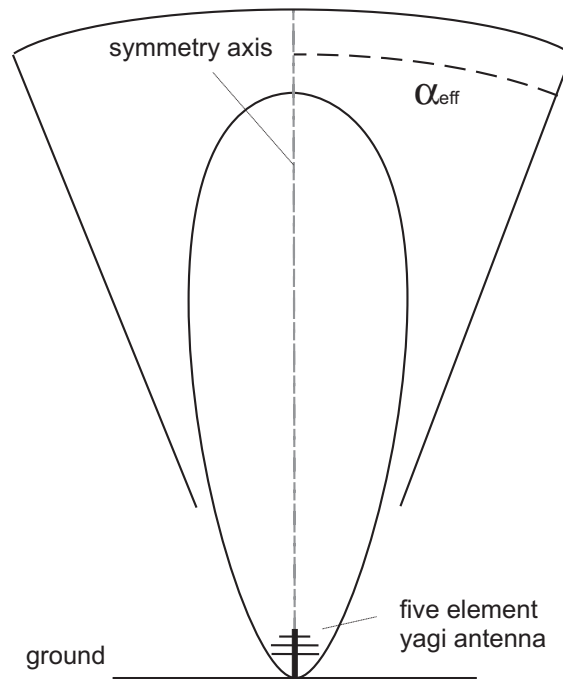


Figure 3: Scheme of the antenna power pattern for a five element Yagi antenna as used for the Collm meteor radar. The effective antenna opening angle  $\alpha$  is defined by the 3dB level.

The insulation of the power fed into the receiver is also necessary to avoid any damage to the hardware due to electrical surge. The red lines in figure 4 mark the injection of the noise generator or the delay line instead of the antenna cables. For the transmitter it is also possible to use a duplexer to separate the signal into two portions, namely for the transmitting antenna and for the delay line. The calibration with the noise generator is also shown in figure 4. In this case the transmitter cables do not have to be interrupted. In fact, a calibrated noise signal is than directly fed into the receivers. However, for the calibration of the Collm (51.3°N, 13°E) radar both methods were applied and the results will be discussed in the next sections. In general, the calibrated noise source can also be the cosmic radiation, but therefore it has to be ensured that no absorption disturbs the measurements during the calibration. Hence, the use of cosmic radiation as noise source is difficult for all wide beam radars operating in the frequency domain from 20 to 40 MHz, which are affected by the same problems than standard Riometers.

#### 4.1 Calibrated noise source

The idea of this calibration method includes the use of a calibrated noise source and feeding this noise directly into the receiver unit of the radar. The noise generator delivers a specified noise in dB. This noise power  $P_{inp}$  can be described similar to the cosmic radiation (equation 1) with a noise temperature  $T_{inp}$ ;

$$P_{inp} = k_B B T_{inp} = c T_{inp} \quad , \quad (6)$$

where  $T_{inp}$  is the equivalent noise temperature. However, the receiver and A/D converter create some noise due to their own noise temperature  $T_r$ . This results in an offset of the measured noise power at the receiver output, which leads to;

$$P_r = g_r k_B B (T_r + T_{inp}) \quad , \quad (7)$$

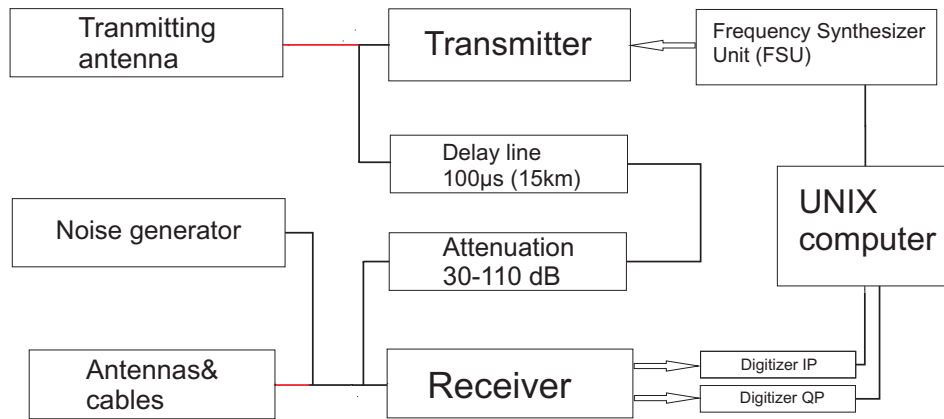


Figure 4: Schematic of the absolute calibration of an VHF radar as done at Collm radar site.

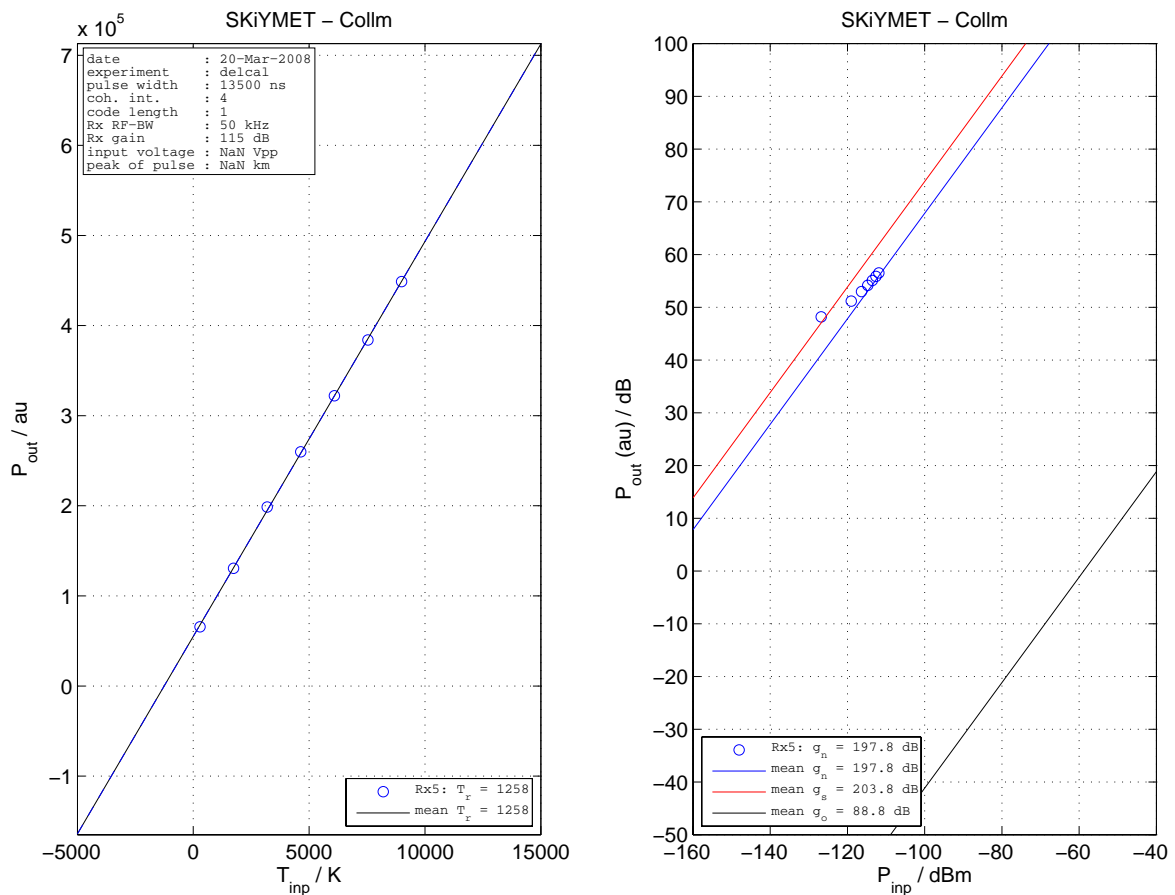


Figure 5: Noise calibration coefficient estimated from calibrated noise source measurements with direct injection into the receiver. Left: graph of receiver output power versus noise temperature as generated from the source to estimate the receiver noise temperature  $T_r$ . Right: receiver input power [dBm] versus output power [dB] as measured during the calibration. Figure provided by IAP Kühlungsborn (courtesy of W. Singer).

where  $g_r$  is the receiver gain for the receiver output power  $P_r$  in arbitrary units ( $au$ ). Equation 7 can be expressed according to Latteck et al. (2008);

$$P_r = a + b \cdot T_{inp} \quad (8)$$

The coefficients  $a$  and  $b$  can be estimated by a linear fit. Using equation 6 and 8 allows to determine the calibration coefficient  $c_i$  for incoherent signals as noise (Latteck et al., 2008);

$$c_i = \frac{P_{inp}}{P_r - a} . \quad (9)$$

However, for coherent signals one has to consider the pulse code length  $n$  as well as the number of coherent integrations  $m$ . Taking these factors into account leads to a calibration coefficient for coherent signals  $c_c$  as described by;

$$c_c = \frac{c_i}{n \cdot m} . \quad (10)$$

This results in the conversion for coherent signals applying the equation for the absolute calibration;

$$P_{inp}[W] = P_r[au] \cdot c_c . \quad (11)$$

In the left panel of figure 5 the application of the outlined procedure to the Collm radar is shown. The offset due to the receiver thermal noise as a noise temperature  $T_r$  is clearly distinguishable. The receiver number five ( $R_{x5}$ ) was taken as representative for all the other receiver channels. In the right panel of figure 5 one can see the connection of the injected noise power into the receiver in  $dBm$  with the measured noise power in  $dB$ . The calibration coefficients given in this case are expressed as a gain in  $dB$ . The labels at gains  $g_{n/s}$  in figure 5 correspond to the calibration coefficients  $c_i$  for incoherent and  $c_c$  for coherent signals. Hence, the calibration constants can be computed from for incoherent signals;

$$g_n[dB] = 10 \cdot \log\left(\frac{P_{inp}[W]}{P_r[au]}\right) = 10 \cdot \log(c_i) , \quad (12)$$

and for coherent signals;

$$g_s[dB] = 10 \cdot \log\left(\frac{P_{inp}[W]}{P_r[au]}\right) = 10 \cdot \log(c_c) . \quad (13)$$

For the Collm radar system the red line in figure 5 marks the coherent calibration curve and the blue line the incoherent calibration curve. The radar uses a 16 bit coded pulse with a 4 point coherent integration.

## 4.2 Delay line method

The calibration with the delay line uses the second branch in the configuration scheme in figure 4. The advantage of this method is that it directly leads to the calibration factor  $c_c$  for coherently received signals (Latteck et al., 2008). In addition, it is possible to process all the five receiver channels parallel to each other. Using a directional coupler allows to measure the exact power of the signal at the transmitter output  $P_{inp}$ , which was created in the FSU. This signal is then directly fed into the delay bridge of  $100 \mu s$ , which simulates a target at approximately  $15 km$  distance at the receiver output (figure 6, left panel). The attenuation cell is necessary to avoid saturation of the receiver and is further used to adjust the receiver output to create variable signal amplitudes. The calibration curve for all channels is shown in figure 6. Here the signal input power at the transmitter is given in  $dBm$  and the receiver output power in  $dB$  for arbitrary units. The calibration coefficient can be estimated by using the following expression according to Latteck et al. (2008);

$$c_c = \frac{P_{inp}[W]}{P_r[au]} . \quad (14)$$

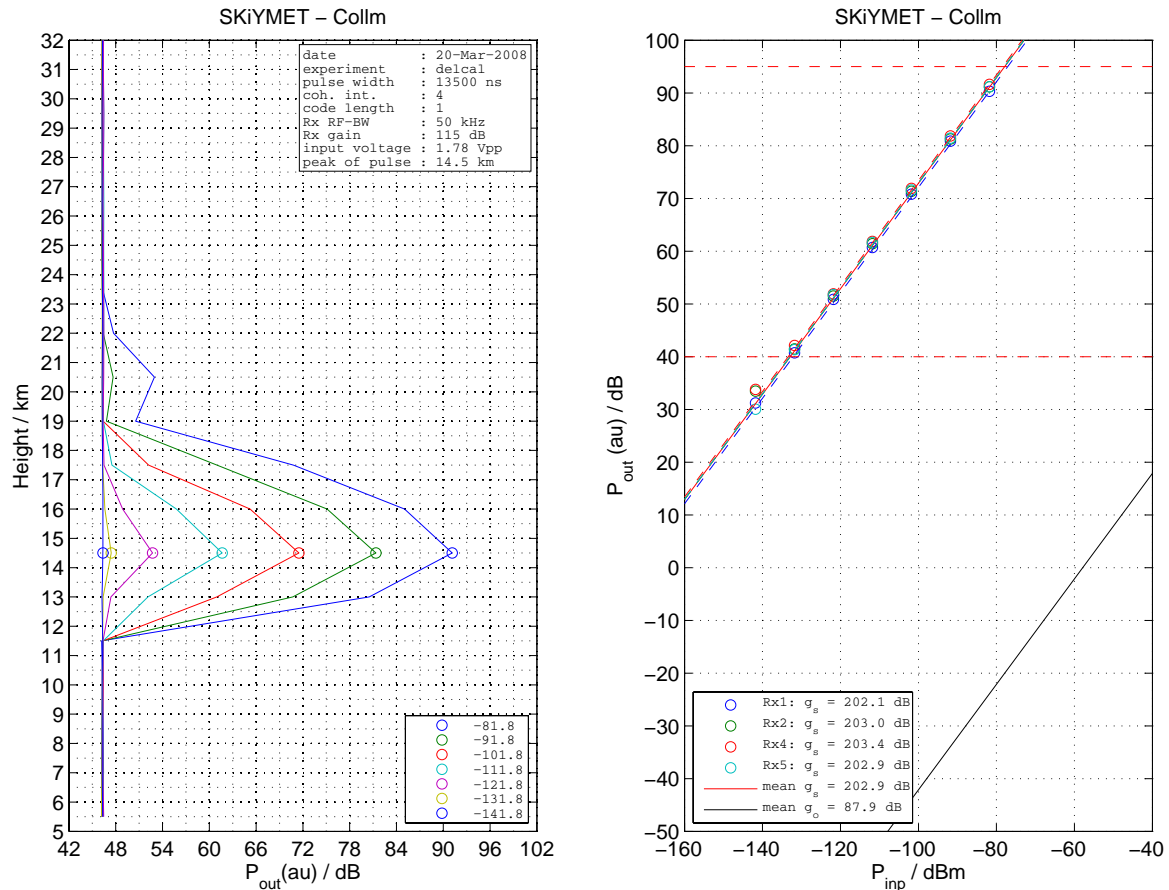


Figure 6: Left: height calibration plot measured with the delay line method. Right: receiver input power [dBm] versus output power [dB] as measured during the calibration. This figure was provided by IAP Kühlungsborn (courtesy of W. Singer).

Another aspect of the delay line calibration is the higher accuracy of the height measurement. In figure 6 (left panel) the amplitude peaks slightly below the 15 km range marker. The reason for this difference of approximately 500 m are the removed antenna cables (figure 4). Thus, this additional antenna cable delay has to be added in the height calibration and then one will end up at 15 km. However, the altitude measurement is much more accurate than the typical size of a range gate of 2 km. In figure 7 both methods are compared and so the good coincidence is visualized. But the plot also reveals the differences between the procedures. The broader range of the measured signal power available due to the variable attenuation cell for the delay line method makes the fit more reliable. Nevertheless, the two introduced procedures lead to almost identical calibration coefficients for coherent signals. For the practical implementation to measure electron line densities from coherent meteor echo signals the returned power  $P_r$  in watts follows from;

$$P_r = c_c \cdot A^2[du] = 4.6 \cdot 10^{-21} \cdot A^2[du] \quad , \quad (15)$$

where  $A$  is the meteor maximum amplitude in digitizer units and  $P_r$  is the corresponding received signal power in watts. The calibration factor  $c_c = 4.6 \cdot 10^{-21}$  is very close to the calibration coefficient for the Andenes SKiYMET meteor radar with  $c_c = 4 \cdot 10^{-21}$  (Singer et al., 2008).

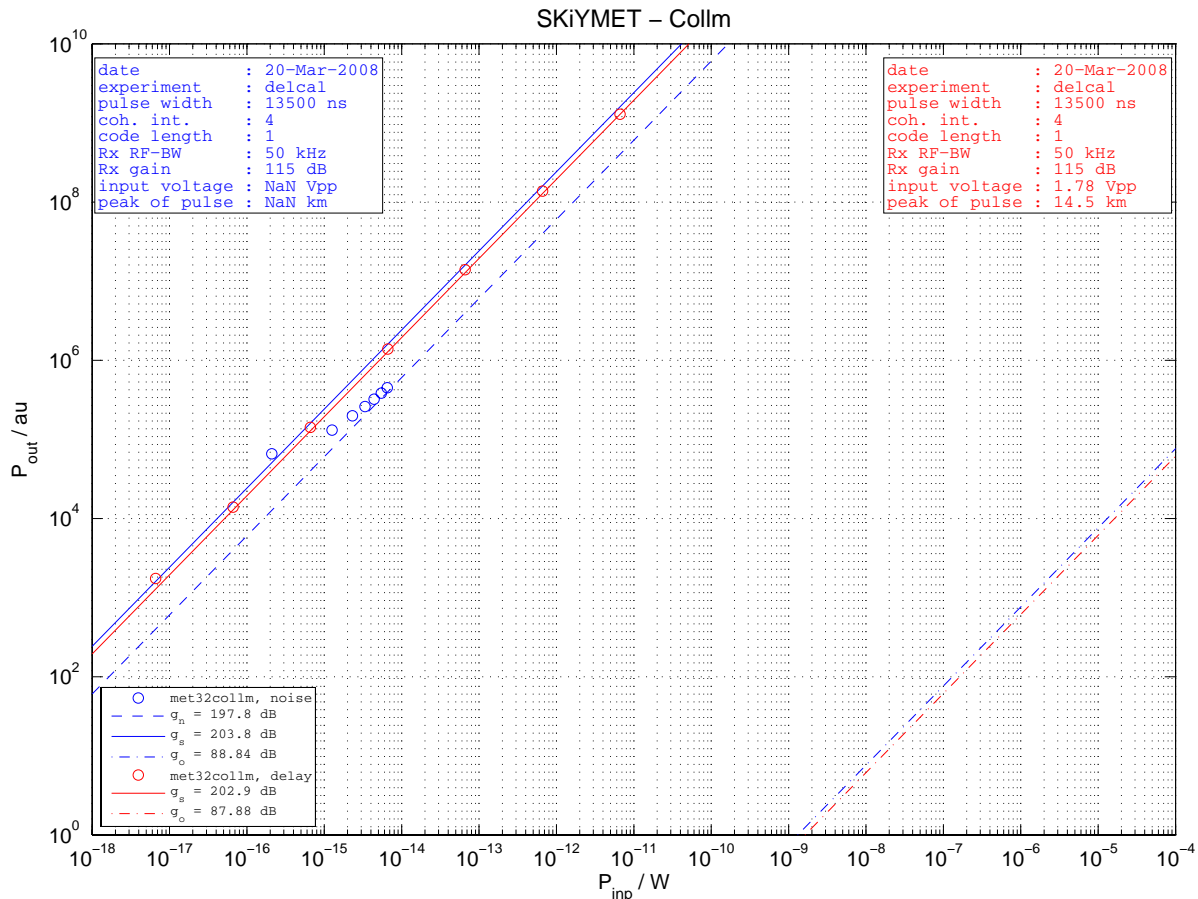


Figure 7: Comparison of the two calibration methods with the calculated calibration coefficients. This figure was provided by IAP Kühlungsborn (courtesy of W. Singer).

### 4.3 Quiet Day Curve

The estimation of the QDC is a challenging task for a mid-latitude station. For polar latitudes (above  $70^\circ$ ) the QDC is determined by measurements during the polar night. The nighttime observation ensures that the absorption is almost zero. For a mid-latitude radar site this procedure is not applicable. The solar activity affects the measurements during each day, because the sun is always for a several hours above the horizon. One possibility to estimate a QDC is to measure one half of the curve in the hemispheric winter during the night and half a year later the other part of the QDC. However, this method is also not very practicable for the mid-latitudes due to the different lengths of day and night between summer and winter. Hence, for the presented results we remove a remaining background absorption from the data by a statistical approach.

The noise measurement is performed during regular operation in meteor mode. For each meteor event the system stores 4 s of data to a so-called CEV-File (Confirmed Event File). These records contain 1 s of data prior to the  $t_0$ -point of the meteor echo and 3 s after it (Hocking et al., 2001). Hence, the file provides also some information about the cosmic noise before and after the meteor event. However, to prevent any difficulties that may arise from measurements of overdense meteor echoes, only the data prior the meteor signal is used. The Collm radar operates with a PRF (Pulse Repetition Frequency) of 2144 Hz and applies a four point coherent integration. Thus, the effective PRF is 536 points for 1 s of raw data. To avoid any problems caused by the  $t_0$  trigger, the noise measurement includes just the first 400 data points of each record. Before this data can

be processed a probable DC offset has to be removed;

$$\begin{aligned} IPm_i &= IP_i - \overline{IP} , \\ QPm_i &= QP_i - \overline{QP} , \end{aligned} \quad (16)$$

where  $\overline{IP}$  and  $\overline{QP}$  are the mean complex values of the receiver and  $IPm_i$  and  $QPm_i$  are the DC offset-free in-phase and quadrature components. This procedure is separately applied to each receiver. Indeed, we use only the two receiver channels with the best signal to noise ratio for the measurements given from the mpd-file (Meteor Position Data). Finally, the amplitude and the variance of the selected points are computed and stored to a noise-file in analogy to the mpd-files. However, the estimation of the QDC requires the removal or suppression of ionospheric absorption or damping of the signal. Therefore, the mean noise amplitude is not an adequate parameter (W. Singer, private communication). A better choice is the upper quantile or decile of the variance above the mean cosmic radiation signal  $A_{quant}$  in arbitrary units. Applying the results derived from the calibration for the coherently integrated signals lead to an extraterrestrial radiation noise power  $P_r$  in watts;

$$P_r = \frac{c_c \cdot A_{quant}^2 \cdot m}{G_{rx}} , \quad (17)$$

where  $c_c$  is the calibration coefficient for coherent signals with a four point integration,  $m$  is the coded pulse length (16 bit) and  $G_{rx}$  is the receiver antenna gain including possible cable losses. For the Collm meteor radar the cable losses are  $L = 1.61 \text{ dB}$ . The directivity of a Yagi antenna is  $D = 5.4 \text{ dB}$  (Singer et al., 2004). Hence, the resultant antenna gain  $G_{rx}$  including antenna directivity and cable losses is  $3.2 \text{ dB}$ .

To reduce the impact from sudden particularities in the cosmic radiation all analyzed meteor records are assigned to a bin according to their sidereal time of occurrence with a resolution of  $10^\circ$ . This allows to derive a noise map for each day by calculating the mean value of each sidereal time bin. The errors of each bin are computed from the fluctuations within the bins. For the estimation of the QDC the data from January 2008 was chosen. During the whole month the day-to-day variability was small. Therefore, the QDC was determined as the average of some quiet days during this time. This procedure results in the QDC shown in figure 8. The cosmic radiation indicates a clear diurnal pattern. This pattern is mainly caused by the radiation of our home galaxy and also carries some information of the antenna pattern.

#### 4.4 Evaluation of the calibration

An evaluation of the quality of the calibration is performed by comparing the observed QDC to a reference QDC derived from a sky temperature map. Unfortunately, cosmic radiation measurements depend on the system parameters as the antenna opening angle  $\alpha_{eff}$ , the radar site (geographic latitude) and the operating frequency. Thus, in literature a number of sky noise observations are published. Nevertheless, only a few of them covered the complete celestial hemisphere and the measurements were done using a broad range of frequencies from  $20 \text{ MHz}$  to several  $\text{GHz}$ . However, for radars operated in the VHF frequency band one of the most suitable sky maps is still the map from Cane (1978) derived at  $30 \text{ MHz}$ . This sky observation covers almost the complete celestial hemisphere from  $\alpha = 0^\circ \dots 360^\circ$  and  $\delta = -85^\circ \dots 85^\circ$ . The grid resolution of the map is  $10^\circ$  in right ascension and  $5^\circ$  in declination.

This reference sky temperatures were measured at  $30 \text{ MHz}$  and have to be converted to the frequency of the Collm radar  $36.2 \text{ MHz}$ . This ensures the comparability between the reference and the observed QDC. A simple expression can be used, which allows

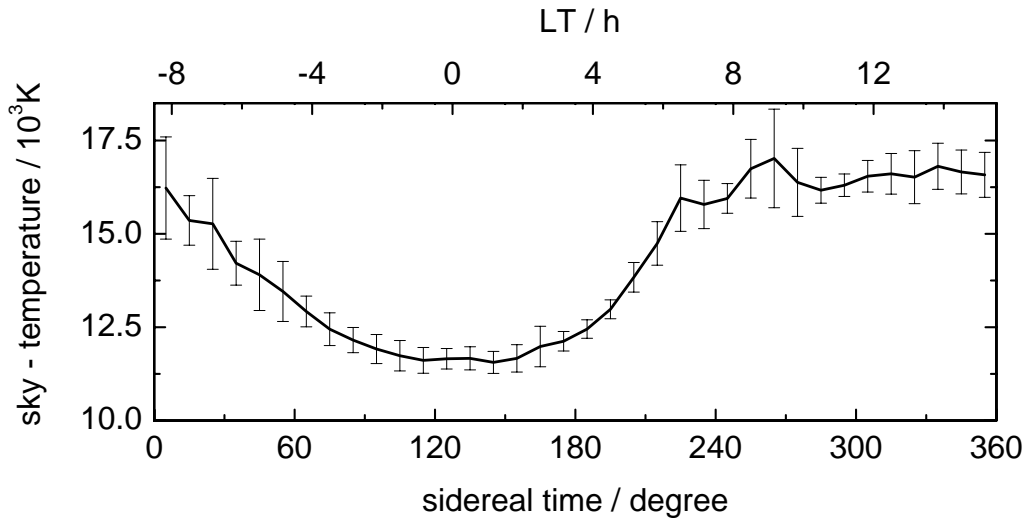


Figure 8: QDC defined by the cosmic radiation measurements during the January 2008 at Collm (51.3° N, 13° E).

to convert an observed sky temperatures  $T_1$  measured at a frequency  $f_1$  to another sky temperature  $T_2$ , which one would expect for a radar operating at frequency  $f_2$ ;

$$\frac{T_1}{T_2} = \left(\frac{f_1}{f_2}\right)^{-\beta_s}, \quad (18)$$

where  $\beta_s$  is the spectral index. This index has typical values ranging from 2.4 to 2.55 and is assumed to be constant over a limited frequency range (Roger et al., 1999). For the results presented here the spectral index is  $\beta_s = 2.5$ . The error caused by using the spectral index as constant is of the order of 100 K.

For the calculation of the QDC from the reference map, the antenna pattern has to be known. The radar at Collm (51.3°N,13°E) is placed on a 7° tilted plane. Additionally, the azimuth calibration has an 2-3° offset from the east reference. In Singer et al. (2004) the antenna pattern for a two element crossed Yagi receiver antenna as used by the SKiYMET radar is given. Such an antenna results in an almost isotropic beam with a 3 – dB opening angle of  $\alpha_{eff} = 54.5^\circ$  (courtesy of Genesis Software). This antenna placed at the Collm radar site (51.3°N, 13°E) would receive cosmic radiation from the area labeled in figure 9 taking a right ascension  $\alpha = 180^\circ$  for the vertical beam. Integrating over the area covered in figure 9 allows to calculate a theoretical QDC for different 3 – dB opening angles ( $\alpha_{eff}$ ). However, the smallest beam width useable is given by the resolution of the lattice, which is approximately  $\alpha_{eff} = 5^\circ$  and further called pencil like beam. In figure 10 the resulting QDC for an isotropic antenna and different beam widths are compared for the Collm radar location. For a pencil like beam the QDC is dominated by two significant peaks, which represent the galactic disc. However, at a right ascension of approximately  $\alpha = 300^\circ$  the most significant radio source (Cygnus A,  $\alpha = 300^\circ, \delta = 40.4^\circ$ ) on the northern hemisphere leads to an increased received noise intensity. From figure 10 it is also obvious that the peak amplitude is reduced for an increasing opening angle  $\alpha_{eff}$  yielding in an diurnal oscillatory pattern of the QDC. Friedrich et al. (2002) did a similar study for Riometers with different opening angles located close to the polar circle and computed the relative absorption in dB. However, a comparison of the results leads to rather similar effects for the simulated half opening angles. Nevertheless, a mid-latitude station shows a larger diurnal variation of the QDC compared to a polar station for the same antenna opening angles. However, in the

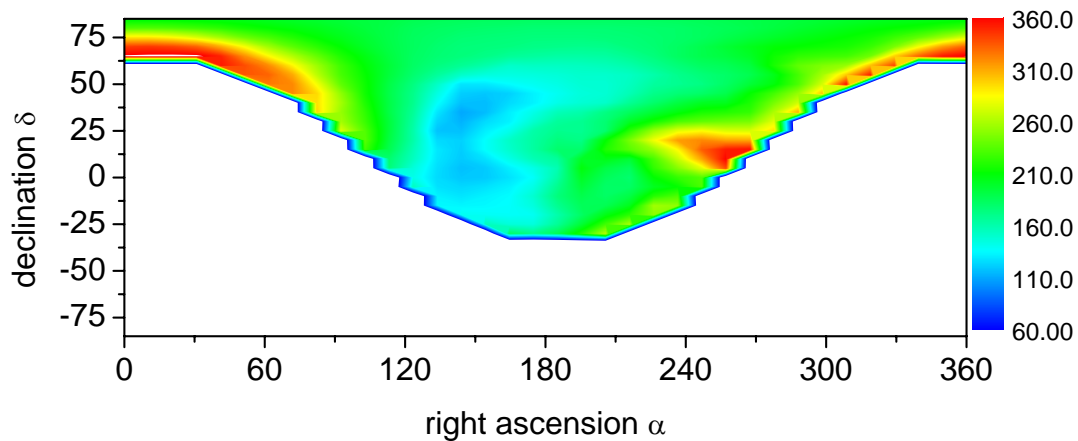


Figure 9: Isotropic (quadrupole) antenna pattern simulated for Collm (51.3°N, 13°E).

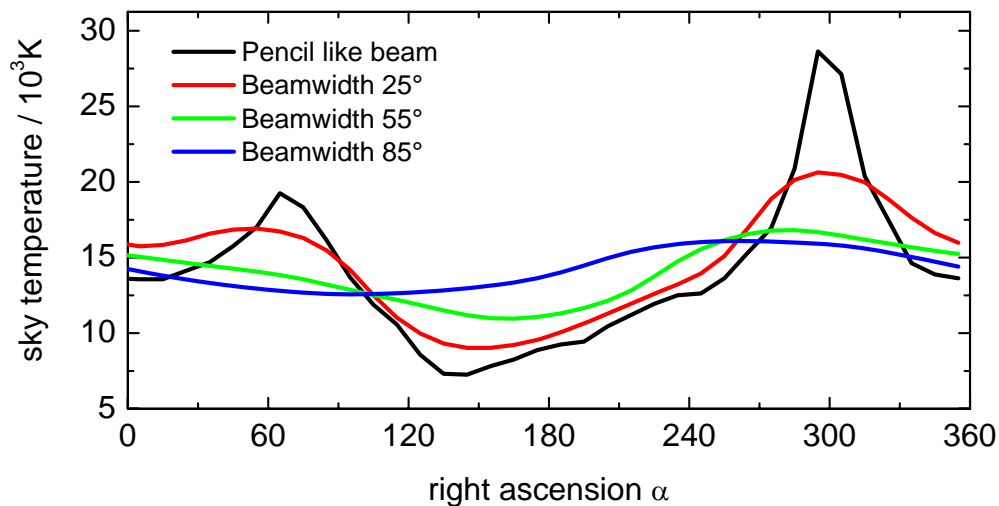


Figure 10: Comparison of different opening angles  $\alpha_{eff}$  for a isotropic antenna pattern.

case of the Collm meteor radar the antenna shows a non-isotropic pattern, and therefore the alignment of the dipole from east to west has an influence on the received cosmic radiation. In figure 11 the dipole characteristics of the antenna is shown for a right ascension  $\alpha = 180^\circ$  and assuming that the  $3 - dB$  beam width has an almost ideal dipole receiver pattern (McKinley, 1961). In fact, the limited resolution of the reference map does not allow to determine the alignment of the antenna with an accuracy better than  $5-7^\circ$ . However, this is still sufficient to study the impact of the alignment. It should also be noted that the coverage of the celestial hemisphere compared to the isotropic pattern (figure 9) is distorted due to the chosen type of projection. This has also to be taken into account for the integration of the beam on the celestial sphere, which is necessary to compute the received noise power. Assuming a dipole antenna pattern as shown in figure 11 enables us to compute the QDC at Collm radar site from the reference sky temperature map. This reference QDC can then be compared to the measured QDC. The coincidence between the measured and computed QDC in figure 12 is remarkable and demonstrates the ability to observe cosmic radiation with reasonable accuracy. Both noise temperature curves show a relative variation of approximately  $1.8 dB$ . The re-

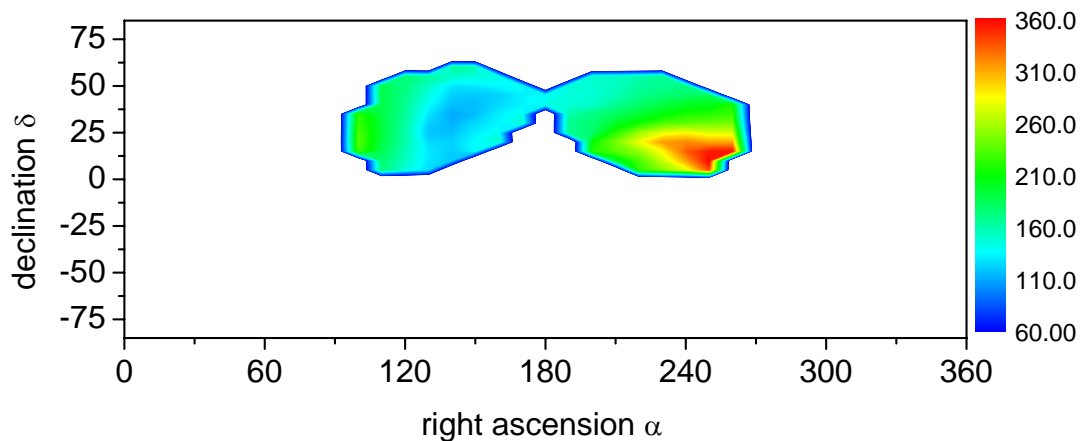


Figure 11: Un-isotropic (Dipol) antenna pattern as used at Collm (51.3°N, 13°E).

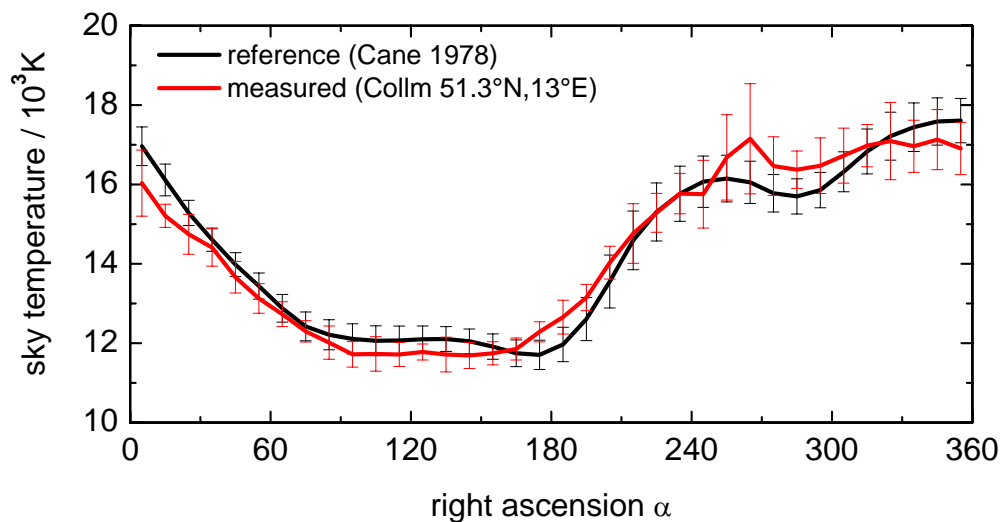


Figure 12: QDC defined by the cosmic radiation measurements during 3-6 January 2008 at Collm (51.3°N, 13°E).

maining differences between both QDC can be explained by the assumptions about the antenna pattern, which was considered to be an ideal dipole. Additionally, atmospheric particularities as, e.g., a non constant absorption during the measurement time in January 2008 may lead to some disturbances in the observed QDC. Finally, also the reference map from Cane (1978) is, due to the limited resolution of  $10^\circ \times 5^\circ$ , not able to reflect all the details for an exact computation of the references curve. In figure 13 the correlation between both QDC demonstrates the very good agreement. The correlation coefficient is  $R = 0.97$  and the offset of  $159\text{ K}$  is smaller than the estimated average error of  $600\text{ K}$ . This error shows the same magnitude than the uncertainty given in Campistron et al. (2001). They derived a partial cosmic noise map using five VHF-ST radars with a beam width of  $6 - 7^\circ$ . Figure 13 further indicates that the slope of the correlation of the two QDC is useable as a first order estimate of the calibration coefficient as done in Stober et al. (2008). However, the so determined calibration coefficient is only valid for incoherent signals (Latteck et al., 2008) and the antenna gain as well as the pattern has to be known. Hence, the comparison of the observed QDC and the reference QDC computed from noise map published by Cane (1978) demonstrates the ability of standard meteor

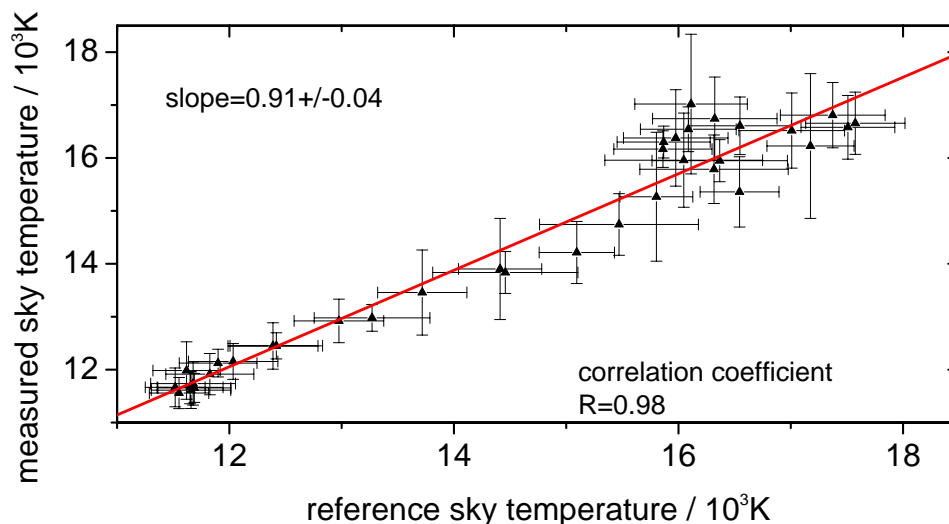


Figure 13: The correlation of QDC measurement during 3-6 January 2008 at Collm (51.3°N, 13°E) and the reference from Cane (1978).

radars to measure cosmic radiation and their variation with acceptable accuracy. In fact, the cosmic noise received by the radar provides a possibility to evaluate the quality of the absolute calibration for a known antenna gain and pattern. A long term observation during the winter 2007/08 indicated a probable ionospheric coupling in dependence of the solar activity. The radar showed a very high stability and no system drift. However, this measurements have to investigated in detail, which could not be done here and is beyond the scope of this paper.

## 5 Conclusion

Two calibration methods, which were applied to the Collm meteor radar (51.3°N, 13°E), were evaluated by studying cosmic noise. The comparison between the two QDC demonstrate the ability to observe cosmic radiation with standard meteor radars. Further, we were able to quantify the impact of the antenna pattern on the resulting noise curves in absolute sky noise temperature values and noise power in watts. In future the results will be used to measure atmospheric absorption for a mid-latitude station. In addition, it was possible to quantify the losses of the antenna gain during the summer period due to the surrounding trees with an additional absorption of 0.5 – 1 dB.

## Acknowledgments

Special thanks to W. Singer in Kühlungsborn for advice, useful discussions and support during the calibration. The technical support and maintenance of the radar at Collm by F. Kaiser is acknowledged.

## References

- Campistron, B., G. Despaux, M. Lothon, V. Klaus, Y. Pointin, and M. Mauprivez, 2001: A partial 45 mhz sky temperature map obtained from the observations of five st radars, *Annales Geophysicae*, 19(8), 863–871.
- Cane, H.V., 1978: A 30 mhz map of the whole sky, *Australien Journal of Physics*, (31):561.
- Friedrich, M., M. Harrich, K.M. Torkar, and P. Stauning, 2002: Quantitative

measurements with wide-beam riometers, *Journal of Atmospheric and Solar-terrestrial Physics*, 64(3), 359–365.

Hocking, W.K., B. Fuller, and B. Vandeppeer, 2001: Real-time determination of meteor-related parameters utilizing modern digital technology, *Journal of Atmospheric and Solar-terrestrial Physics*, 63(2-3), 155–169.

Latteck, R., W. Singer, R.J. Morris, W.K. Hocking, D.J. Murphy, D.A. Holdsworth, and N. Swarnalingam, 2008: Similarities and differences in polar mesosphere summer echoes observed in the arctic and antarctica, *Annales Geophysicae*, 26, 2795–2806.

Roger, R.S., C.H. Costain, T.L. Landecker, and C.M. Swerdlyk, 1999: The radio emission from the galaxy at 22 Mhz, *Astron. Astro-phys. Suppl.*, 137, 7–19.

Singer, W., R. Latteck, L.F. Millan, N.J. Mitchell, and J. Fiedler, 2008: Radar backscatter from underdense meteors and diffusion rates, *Earth Moon and Planets*, 102(1- 4), 403–409.

Singer, W., U. von Zahn, and J. Weiss, 2004: Diurnal and annual variations of meteor rates at the arctic circle, *Atmospheric Chemistry and Physics*, 4, 1355–1363.

Stober, G. and Ch. Jacobi, 2008: Electron line densities and meteor masses calculated from models and meteor radar measurements, *Rep. Inst. Meteorol. Univ. Leipzig*, 42, 155–168.

#### **Addresses of Authors:**

Gunter Stober, Institute for Meteorology, University of Leipzig, Stephanstr. 3, 04103 Leipzig, [stober@uni-leipzig.de](mailto:stober@uni-leipzig.de)

Christoph Jacobi, Institute for Meteorology, University of Leipzig, Stephanstr. 3, 04103 Leipzig